IOPscience iopscience.iop.org

Home Search Collections Journals About Contact us My IOPscience

Changes in the spin-glass state and the atomic structure on annealing the amorphous Y - Fe alloys

This article has been downloaded from IOPscience. Please scroll down to see the full text article.

1996 J. Phys.: Condens. Matter 8 2219

(http://iopscience.iop.org/0953-8984/8/13/013)

View the table of contents for this issue, or go to the journal homepage for more

Download details:
IP Address: 171.66.16.208
The article was downloaded on 13/05/2010 at 16:27

Please note that terms and conditions apply.

J. Phys.: Condens. Matter **8** (1996) 2219–2231. Printed in the UK

Changes in the spin-glass state and the atomic structure on annealing the amorphous Y–Fe alloys

T Suzuki†, A Fujita†, K Fukamichi†, H Aruga-Katori‡, T Goto‡, M Hashikura†, E Matsubara§ and Y Waseda‖

† Department of Materials Science, Faculty of Engineering, Tohoku University, Sendai 980–77, Japan

‡ Institute for Solid State Physics, University of Tokyo, Roppongi 106, Japan

§ Department of Metallurgy, Faculty of Engineering, Kyoto University, Kyoto 606, Japan

‖ Institute for Advanced Materials Processing, Tohoku University, Sendai 980-77, Japan

Received 5 May 1995, in final form 15 August 1995

Abstract. Annealed amorphous Y_xFe_{100-x} alloys have been investigated by means of AC magnetic susceptibility measurement and x-ray diffraction analysis. The amorphous Y_xFe_{100-x} ($x = 15$, 16, 20, 25 and 30) alloys annealed at 523 K for 180 min exhibit re-entrant spin-glass behaviour, while a direct transition from a paramagnetic to a spin-glass phase occurs in the amorphous alloys with $x = 7.5$, 10 and 33.3. For the amorphous $Y_{20}Fe_{80}$ alloy, the Curie temperature and the magnetic moment increase, but the spin freezing temperature decreases on annealing. The magnetic phase diagram for the amorphous Y–Fe alloy system in the annealed state is similar to that for many other amorphous Fe-based alloy systems in the as-prepared state. Increases in the atomic distance of Fe–Fe pairs and in the coordination number of the nearest-neighbour Fe atoms on annealing have been observed. These structural changes explain the changes in the magnetic properties for annealed amorphous alloys.

1. Introduction

Amorphous Fe-based alloys with non-magnetic early transition or rare-earth metals exhibit a wide variety of magnetic properties. For amorphous Zr_xFe_{100-x} alloys, the ferromagnetic state appears and the maximum Curie temperature is close to room temperature at around $x = 20$. With decreasing x, the Curie temperature rapidly decreases and a spin-glass state emerges at low temperatures (Fukamichi *et al* 1989). Amorphous M–Fe (M ≡ Zr, Sc, Hf, Ce or Lu) alloy systems exhibit re-entrant spin-glass behaviour (Wakabayashi *et al* 1990, Fukamichi *et al* 1986, 1989, Hiroyoshi *et al* 1985). The Curie temperatures of these systems show a maximum at around $x = 15$–20, while the spin freezing temperatures show a minimum at around similar concentrations (Fukamichi *et al* 1989). It is noteworthy that the spin freezing temperature is about 100 K irrespective of the kind of M element, showing that the spin-glass behaviour comes from the magnetic properties of Fe.

The magnetic properties and the Mössbauer effect for amorphous Y_xFe_{100-x} alloys have been investigated extensively (Chappert *et al* 1981, Coey *et al* 1981). No ferromagnetic state has been observed in the entire concentration range. Therefore, the amorphous Y–Fe alloy system is unique and it is interesting to investigate whether the magnetic properties for the amorphous Y_xFe_{100-x} alloys are essentially different from those for the other amorphous Fe-based alloy systems mentioned above. Recently, it has been reported that amorphous

0953-8984/96/132219+13$19.50 © 1996 IOP Publishing Ltd

Y_xFe_{100-x} alloys exhibit re-entrant spin-glass behaviour in a weak magnetic field, suggesting that the magnetic state in this amorphous alloy system is very close to ferromagnetism (Fujita *et al* 1993). More recently, it has been pointed out that the ferromagnetic state is stabilized by annealing (Suzuki *et al* 1994b). Therefore, a marked difference is expected to occur between the magnetic properties of the annealed and the as-prepared amorphous Y_xFe_{100-x} alloys.

Generally, the heat treatment of amorphous alloys at a temperature lower than the crystalline temperature causes the rearrangement of atoms, resulting in a steadier state. It has been observed that the magnetic properties of amorphous Fe-based alloys are very sensitive to local environments such as the Fe–Fe interatomic distance and the number of the nearest-neighbour Fe atoms (Chiang *et al* 1994, Terashima *et al* 1995). It is, therefore, important to investigate the magnetic and structural properties, especially the magnetic phase diagram and the local environment, for annealed amorphous Y_xFe_{100-x} alloys. It has been reported that the spin freezing temperature is easily reduced by an external magnetic field (Fujita *et al* 1993, Suzuki *et al* 1994b), and hence the spin freezing temperature should be measured in as weak a magnetic field as possible. Moreover, in order to obtain the spin freezing temperature, the measurement of the responses of spins to the AC magnetic field is profitable. Accordingly, the AC magnetic susceptibility measurement in a very weak magnetic field is efficient for obtaining the magnetic phase diagram.

In the present paper, DC and AC field measurements have been reported for as-prepared and annealed amorphous Y_xFe_{100-x} alloys in order to investigate the annealing effect. Furthermore, the relation between the magnetic properties and the structural change on annealing has been discussed.

2. Experimental details

AmorphousY_xFe_{100-x} alloys ($x = 7.5$, 10, 15, 16, 20, 25, 30 and 33.3) were prepared by a high-rate DC sputtering technique on a Cu substrate using alloy targets of 40 mm diameter made by arc melting in an Ar atmosphere. The Ar gas pressure during sputtering was 40 mTorr, and the target voltage and anode current were 1.0 kV and 6.0 A, respectively. The sputtering was continuously carried out for about 2.5 d in order to obtain specimens of thickness about 0.2 mm. The Cu substrate was ground using a wheel. The specimens were annealed *in vacuo*.

Measurement of the AC magnetic susceptibility was carried out by a mutual induction method at a frequency of 80 Hz in an AC magnetic field of 1 Oe. Magnetization up to 5.5 T was measured with a SQUID magnetometer. The high-field magnetization up to near 40 T was also measured by an induction method in pulsed magnetic fields in order to discuss the saturation magnetization.

The amorphous state of the specimens before and after annealing was confirmed by diffraction with monochromatic Mo Kα radiation. The scattering intensity was detected with a pure Ge solid state detector. The elastic scattering intensity was separated from the Y Kα fluorescent radiation. The Y Kβ fluorescence overlapping with elastic scattering was evaluated using the observed Y Kα intensity and the tabulated ratio of Y Kβ to Y Kα (Rao *et al* 1986) in order to correct the elastic scattering. The room-temperature density was obtained by the Archimedean method using toluene as the working fluid.

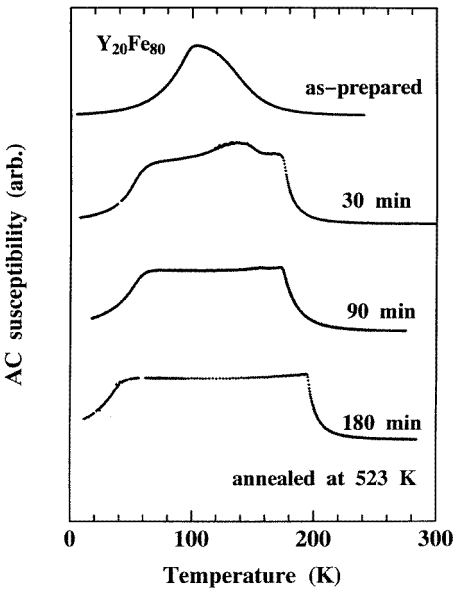

Figure 1. Temperature dependence of the AC magnetic susceptibility for the amorphous $Y_{20}Fe_{80}$ alloys annealed at 523 K for 30, 90 and 180 min, together with that for the as-prepared alloy.

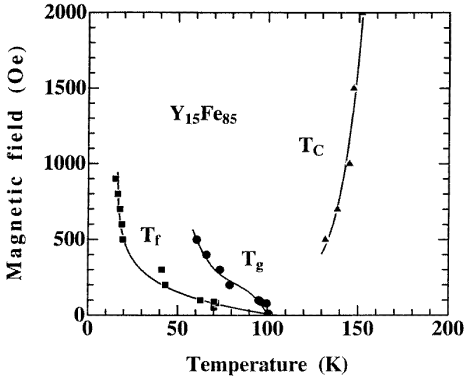

Figure 2. The magnetic field dependence of the transition temperatures for as-prepared amorphous $Y_{15}Fe_{85}$ alloy. The two types of freezing temperature are indicated by T_g and T_f and the Curie temperature by T_C.

3. Results and discussion

All the annealed Y_xFe_{100-x} specimens have been confirmed to be amorphous by x-ray diffraction. Figure 1 shows the temperature dependence of the AC magnetic susceptibility for the amorphous $Y_{20}Fe_{80}$ alloys annealed at 523 K for 30, 90 and 180 min, together with that of the as-prepared alloy, for comparison. The last alloy exhibits only one peak at around 100 K, being characteristic of a paramagnetic–spin-glass transition. However, the annealed specimens show a rapid increase at around 180–200 K (which indicates the emergence of a ferromagnetic state with decreasing temperature) and a decrease at around 40–60 K due to re-entrant behaviour. From these results, it is clear that the ferromagnetic state appears after annealing. For the specimen annealed for 30 min, another small broad peak appears at around 140 K. This behaviour is connected with a heterogeneous structural relaxation. The specimen annealed for 90 min still has a very small peak at around 160 K, and eventually this small peak disappears after annealing for 180 min. The very flat temperature dependence is caused by the demagnetization effect. It should be noted that the Curie temperature shifts to a higher temperature but the spin freezing temperature shifts to a lower temperature on increase in the annealing time. These facts indicate that the ferromagnetic state is gradually stabilized with respect to annealing time.

Figure 2 shows the magnetic field dependences of the Curie temperature T_C and two types of spin freezing temperature, namely T_g and T_f (H–T diagram), determined by means of the differential magnetic susceptibility measurement for the as-prepared amorphous $Y_{15}Fe_{85}$ alloy. Similar H–T diagrams for amorphous $Y_{16}Fe_{84}$ and $Y_{20}Fe_{80}$ alloys have been reported (Fujita *et al* 1993). In a weak external magnetic field, two types of spin freezing temperature are observed. The higher temperature T_g is considered to be the

freezing temperature of the transverse component of spins, while the lower temperature T_f may correspond to a crossover point from the weakly to the strongly irreversible state. In the strong external magnetic field, the ferromagnetic phase appears between the Curie temperature T_C and the spin freezing temperature T_f. What should be evident is that the temperature T_g becomes vague just before or after the appearance of the Curie temperature T_C. These characteristics of T_C and T_g may not be due to the external magnetic field but may be an intrinsic feature in the re-entrant spin-glass state for amorphous Fe-based alloys. For instance, the change corresponding to T_g is very uncertain while a sharp peak appears at T_f in the differential magnetic susceptibility for amorphous $La(Fe_{0.90}Al_{0.10})_{13}$ alloy, which exhibits re-entrant spin-glass behaviour in a zero magnetic field (Fukamichi *et al* 1995). Considering these facts, the spin freezing temperature of the annealed amorphous $Y_{20}Fe_{80}$ alloy with re-entrant spin-glass behaviour is referred to as T_f. For the as-prepared specimen, the two types of transition occur at the same time in zero magnetic field; therefore the spin freezing temperature T_f coincides with T_g, which corresponds to the cusp in the curve of AC magnetic susceptibility.

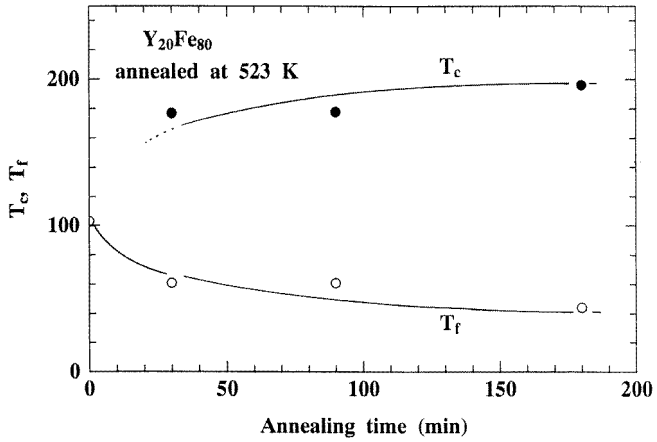

Figure 3. The magnetic transition temperatures versus the annealing time for the amorphous $Y_{20}Fe_{80}$ alloy annealed at 523 K.

The Curie temperature T_C and the spin freezing temperature T_f versus the annealing time for the amorphous $Y_{20}Fe_{80}$ alloy are summarized in figure 3. From these results, the stabilization of the ferromagnetic state seems to be almost established within about 30 min. It is considered that such changes in the magnetic phases are correlated to the change in the local environment of Fe atoms, which is induced by structural relaxation, because the magnetic properties of Fe are sensitive to the distance and the coordination number of neighbouring Fe atoms. Therefore, not only isochronal but also isothermal annealing should cause the change in the magnetic properties of amorphous Y–Fe alloys. Figure 4 displays the temperature dependence of the AC magnetic susceptibility for the amorphous $Y_{20}Fe_{80}$ alloy annealed for 30 min at various temperatures. Stabilization of the ferromagnetic phase and suppression of the spin-glass occur with increasing annealing temperature. After annealing for 30 min at 873 K, consequently, the spin freezing temperature appears below 10 K and the Curie temperature lies just below room temperature. The magnetic transition temperatures versus the annealing temperature for the amorphous $Y_{20}Fe_{80}$ alloy annealed for 30 min are plotted in figure 5. The change in the magnetic phase is sluggish for the specimen annealed

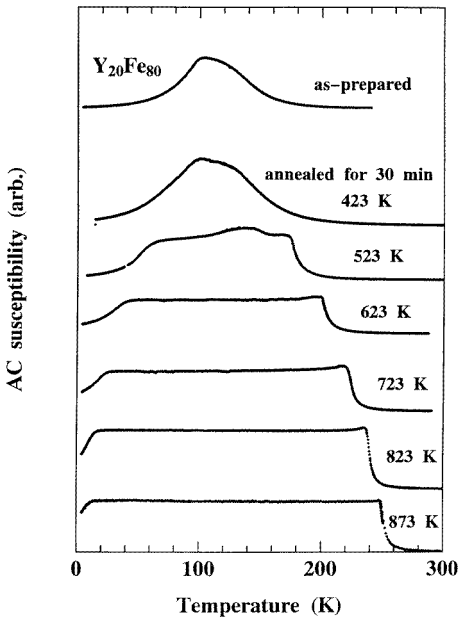

Figure 4. Temperature dependence of the AC magnetic susceptibility for the amorphous $Y_{20}Fe_{80}$ alloys annealed at various temperatures for 30 min, together with that for the as-prepared alloy.

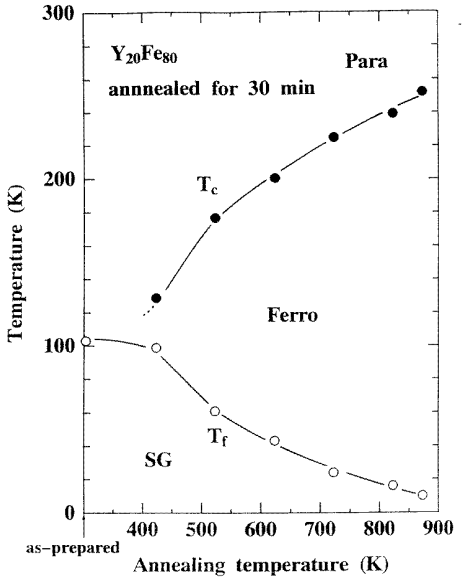

Figure 5. The magnetic transition temperatures versus the annealing temperature for the amorphous $Y_{20}Fe_{80}$ alloy annealed for 30 min.

below 400 K. With increasing annealing temperature, the Curie temperature increases and the spin freezing temperature decreases.

The ferromagnetic state is also confirmed in the annealed amorphous $Y_{16}Fe_{84}$ and $Y_{25}Fe_{75}$ alloys in a similar manner to the annealed amorphous $Y_{20}Fe_{80}$ alloys, although the Curie temperatures of both alloys are lower than that for the annealed amorphous $Y_{20}Fe_{80}$ alloy. The spin freezing temperature also shifts to lower temperatures for both alloys. Contrary to the Curie temperature, the spin freezing temperatures of the annealed amorphous $Y_{16}Fe_{84}$ and $Y_{25}Fe_{75}$ alloys are higher than that for the annealed amorphous $Y_{20}Fe_{80}$ alloy.

Figure 6 shows the temperature dependence of AC magnetic susceptibility for the amorphous $Y_{15}Fe_{85}$ alloys annealed at 523 K for 30 and 180 min. The result for the as-prepared specimen is given in the same figure. The alloy annealed for 30 min shows a broad peak around 120 K, which is correlated with the appearance of the re-entrant spin-glass state although the as-prepared specimen exhibits a cusp at around 100 K. It is worth noting that the spin freezing temperature shifts to a higher temperature with increasing annealing time as seen from the curve for the alloy annealed for 180 min. Figure 7 shows the temperature dependence of the AC magnetic susceptibility for the amorphous $Y_{30}Fe_{70}$ alloy annealed at 523 K for 30 min, together with that for the as-prepared counterpart, for comparison. The annealed specimen also exhibits the emergence of the ferromagnetic state, and the spin freezing temperature shifts to a higher temperature by about 20 K.

Figure 8 shows the temperature dependence of AC magnetic susceptibility for the amorphous $Y_{10}Fe_{90}$ alloys annealed at 523 K for 30, 90 and 180 min, together with that for the as-prepared specimen, for comparison. It should be noted that these alloys behave in

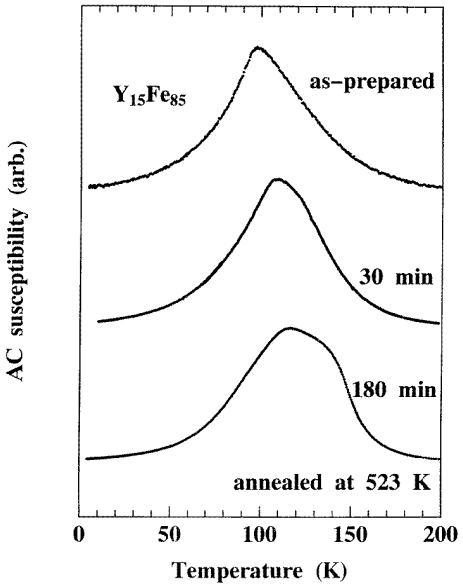

Figure 6. Temperature dependence of the AC magnetic susceptibility for the amorphous $Y_{15}Fe_{85}$ alloys annealed at 523 K for 30 and 180 min, together with that for the as-prepared specimen.

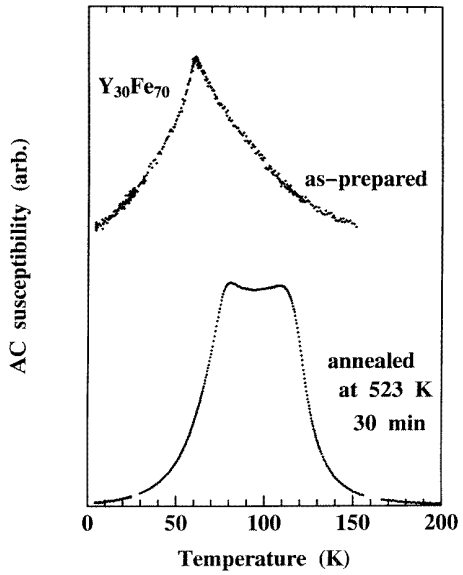

Figure 7. Temperature dependence of the AC magnetic susceptibility for the amorphous $Y_{30}Fe_{70}$ alloy annealed at 523 K for 30 min, together with that for the as-prepared alloy.

another way in contrast with the annealed amorphous alloys mentioned above, i.e. the spin freezing temperature exhibits only a slight shift to a higher temperature. Furthermore, it should be emphasized that the annealed specimens indicate no ferromagnetic state, keeping a clear paramagnetic–spin-glass transition. Figures 9 and 10 show the temperature dependences of AC magnetic susceptibility for the amorphous $Y_{7.5}Fe_{92.5}$ alloy annealed at 523 K for 30 min, and the amorphous $Y_{33.3}Fe_{66.7}$ alloy annealed at 523 K for 180 min, respectively, together with those of the as-prepared counterparts. The annealing effects on the magnetic properties for these alloys are similar to those for the annealed amorphous $Y_{10}Fe_{90}$ alloys, namely no ferromagnetic state but a slight increase in the spin freezing temperature is observed.

From the annealing effects shown in figure 1 and figures 6–10, the change in the transition temperatures is given in the magnetic phase diagram as shown in figure 11. The solid line and dotted line represent the Curie temperature T_C and the spin freezing temperature T_f, respectively, for the specimen annealed at 523 K for 180 min. The spin freezing temperatures T_g for as-prepared specimens are also indicated by the chain line, for comparison (Fukamichi *et al* 1989). Re-entrant spin-glass behaviour appears in the annealed amorphous $Y_{16}Fe_{84}$, $Y_{20}Fe_{80}$ and $Y_{25}Fe_{75}$ alloys. In these alloys, the spin freezing temperature lies in the lower-temperature region, compared with the as-prepared specimen. The annealed $Y_{15}Fe_{85}$ and $Y_{30}Fe_{70}$ alloys are also of re-entrant spin-glass type; however, the spin freezing temperature shifts to a higher temperature. For the annealed amorphous $Y_{7.5}Fe_{92.5}$, $Y_{10}Fe_{90}$ and $Y_{33.3}Fe_{66.7}$ alloys, a paramagnetic–spin-glass transition persists, although the spin freezing temperature shifts to a slightly higher temperature. It should be noted that the present magnetic phase diagram is very similar to those for other many amorphous Fe-based alloy systems such as La–Fe, Ce–Fe and Lu–Fe (Fukamichi

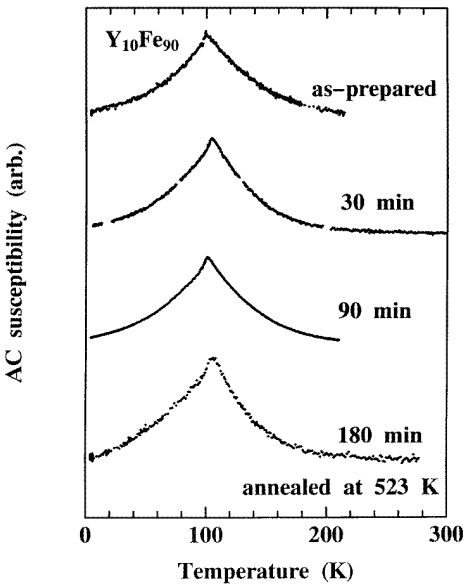

Figure 8. Temperature dependence of the AC magnetic susceptibility for the amorphous $Y_{10}Fe_{90}$ alloys annealed at 523 K for 30, 90 and 180 min, together with that for the as-prepared alloy.

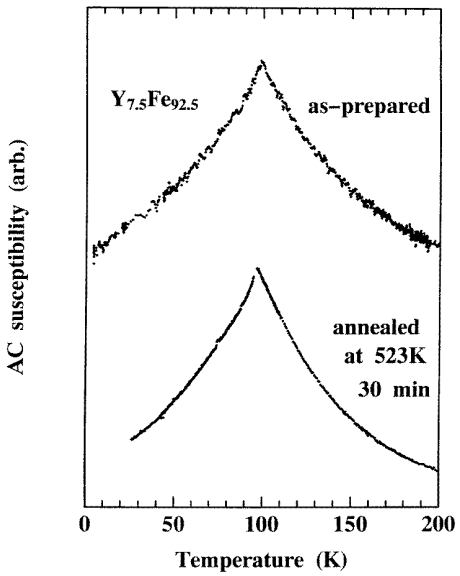

Figure 9. Temperature dependence of the AC magnetic susceptibility for the amorphous $Y_{7.5}Fe_{92.5}$ alloy annealed at 523 K for 30 min, together with that for the as-prepared alloy.

et al 1989). Therefore, the magnetic properties for the amorphous Y–Fe alloy system are essentially regarded as the same as those for many other amorphous Fe-based alloy systems, although the as-prepared amorphous Y–Fe alloys look unique at first glance.

Since pronounced changes in the magnetic phase diagram on annealing are detected by the AC magnetic susceptibility measurement, a change in the magnetization curves is expected. Generally, the magnetization curve of spin glasses is not easily saturated by weak magnetic fields due to the competition between ferromagnetic and antiferromagnetic interactions; therefore, we need very-high-magnetic-field measurements in order to investigate the magnetic properties in detail. Figure 12 shows the magnetization curves up to 40 T at 4.2 K for the amorphous $Y_{20}Fe_{80}$ alloys annealed at 523 K for 30 and 180 min and at 623 K for 30 min, together with that for the as-prepared counterpart for comparison. The saturation of the magnetization gradually becomes easier on increase in the annealing time, indicating a larger magnetization. Swifter changes are caused by higher-temperature annealing. However, it is difficult to evaluate an accurate saturation magnetization. In order to obtain the saturation magnetic moment, the magnetization curves are fitted using the following expression (Fähnle and Kronmüller 1978, Chudnovsky *et al* 1986):

$$M(H) = M_s(1 - a/H^n)\chi_{hf}H \tag{1}$$

where M_s is the saturation magnetization. The high-field magnetic susceptibility χ_{hf} mainly comes from the Zeeman splitting of the d bands due to external magnetic field (Fähnle and Kronmüller 1978, Chudnovsky *et al* 1986). The powers n in the term a/H^n are different depending on the origin, and n for cluster spin glasses becomes 1/2 (Chudnovsky *et al* 1986). The magnetic moment μ_{Fe} per Fe atom obtained from M_s and the factor a versus the annealing time for the amorphous $Y_{20}Fe_{80}$ alloy are displayed in figure 13. The Fe magnetic moment increases with increase in the annealing time. The factor a is regarded

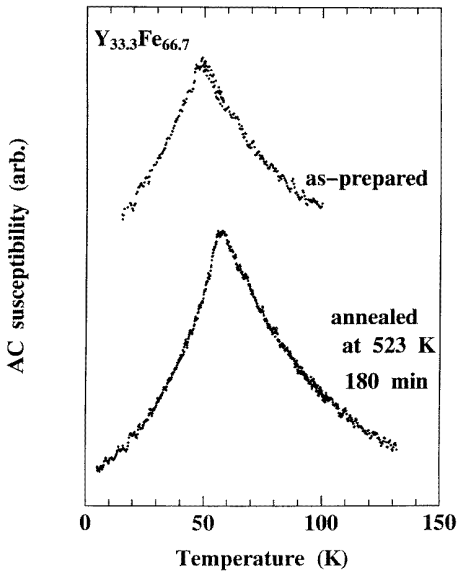

Figure 10. Temperature dependence of the AC magnetic susceptibility for the amorphous $Y_{33.3}Fe_{66.7}$ alloy annealed at 523 K for 180 min, together with that for the as-prepared alloy.

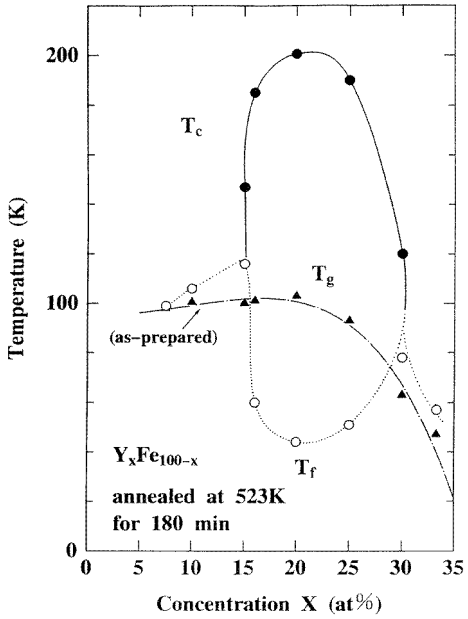

Figure 11. The magnetic phase diagram for the annealed amorphous Y_xFe_{100-x} alloys annealed at 523 K for 180 min. The solid line and dotted line indicate the Curie temperature T_C and the spin freezing temperature T_f, respectively. The data for as-prepared specimens are also shown by the chain line (Fukamichi *et al* 1989), for comparison.

as a measure of the deviation from the long-range ferromagnetic alignment of spins. The factor a decreases with increasing annealing time, indicating an increase in the ferromagnetic interactions. These behaviours exhibit stability of the ferromagnetic state and are consistent with the results obtained from the AC magnetic susceptibility measurements. It is interesting to investigate the change in the magnetization curve on annealing for the amorphous $Y_{10}Fe_{90}$ alloy which has only a slight difference between the spin freezing temperatures of the annealed and the as-prepared specimens as seen in figure 8. Figure 14 shows the magnetization curve for the amorphous $Y_{10}Fe_{90}$ alloy annealed for 30 min, together with that for the as-prepared specimen. The parameters μ_{Fe}, a and χ_{hf} obtained from equation (1) are listed in table 1. At first glance, the magnetization of the former is larger than that of the latter. However, the saturation magnetization M_s obtained from the fitting for the annealed specimen is scarcely different from that for the as-prepared specimen, consistent with the data obtained by the AC susceptibility measurement mentioned before. On the other hand, the factor a and the high-field susceptibility χ_{hf} are changed drastically by annealing. Although the re-entrant behaviour does not appear after annealing, the changes in a and χ_{hf} indicate that the ferromagnetic interaction is relatively stabilized by annealing.

The magnetic properties of amorphous Fe-based alloys with a non-magnetic element are considered to originate from the 3d electrons of Fe. The appearance of the spin-glass phase in the ground state and re-entrant behaviour at finite temperatures for amorphous Fe-based alloys have been discussed on the basis of the theory for itinerant-electron magnetism and spin fluctuations (Kakehashi 1991, 1993). Large spontaneous volume magnetostrictions

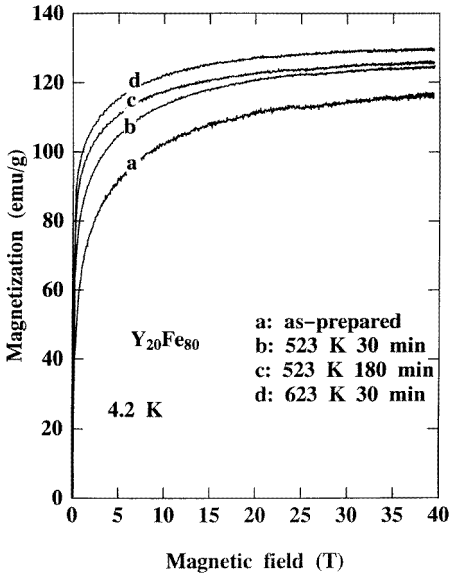

Figure 12. Magnetization curves up to 40 T at 4.2 K for the amorphous $Y_{20}Fe_{80}$ alloys annealed at 523 K for 30 and 180 min and at 623 K for 30 min, together with that for the as-prepared counterpart.

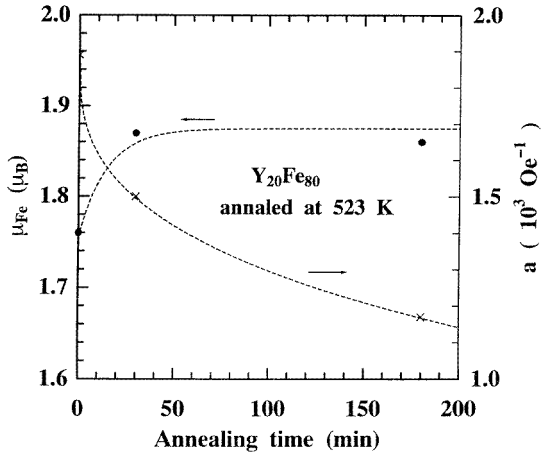

Figure 13. The magnetic moment μ_{Fe} and the factor a in the terms of law of approach to saturation versus the annealing time for the amorphous $Y_{20}Fe_{80}$ alloy.

have been observed for the amorphous Y–Fe alloy system, which is evidence of the strong fluctuations in the local moment of Fe (Fujita *et al* 1994, Suzuki *et al* 1994a). The change in the magnetic state on annealing for the amorphous Y–Fe alloy system should be attributed to the change in the local environment of Fe, because the structural change is reflected in the width of bands and the exchange interactions of 3d electrons. The interference functions of the amorphous $Y_{20}Fe_{80}$ alloys before and after annealing at 523 K for 180 min are compared in figure 15. A slight shift in the oscillations in the interference functions at a

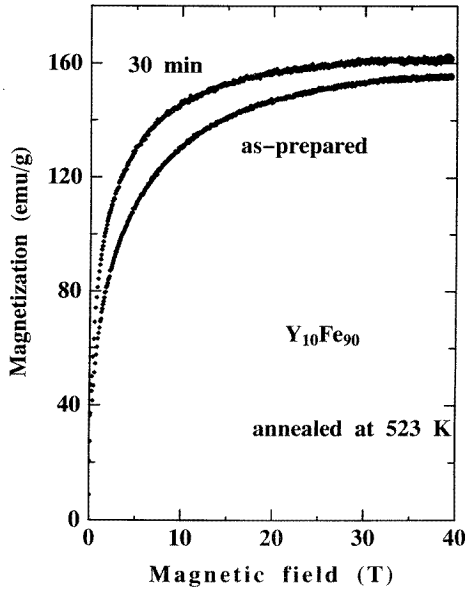

Figure 14. Magnetization curves up to 40 T at 4.2 K for the amorphous $Y_{10}Fe_{90}$ alloys in the as-prepared state and the annealed state at 523 K for 30 min.

high Q-value for the annealed specimen suggests a change in the near-neighbour region. In figure 16 are the radial distribution functions obtained by the Fourier transformation of the interference functions in figure 15. Referring to the atomic radius of each element (Fe, 0.126 nm; Y, 0.178 nm), the peaks and their shoulder in the near-neighbour region are attributed to Fe–Fe, Y–Fe and Y–Y pairs. Their relative peak heights and positions for the annealed specimen are quite different from those for the as-prepared specimen. This indicates that the environmental structure of the nearest neighbour is changed by annealing. In order to evaluate the structural parameters, least-square fitting has been carried out using the procedure proposed previously (Matsubara *et al* 1992). The coordination numbers and the atomic distances for these peaks are summarized in table 2. The atomic distance of the Fe–Fe pairs increases about 2% and the coordination number of the Fe–Fe pairs increases in contrast with decrease in the atomic distance and the coordination number of the Y–Y pairs by annealing.

Table 1. The magnetic moment μ_{Fe}, the factor a and the high-field susceptibility χ_{hf} in terms of the law of approach to saturation for the annealed and as-prepared amorphous $Y_{10}Fe_{90}$ alloys.

	μ_{Fe} (μ_B/Fe atom)	a ($Oe^{1/2}$)	χ_{hf} (10^{-6} emu $g^{-1}Oe^{-1}$)
As prepared	2.0	88	8.82
Annealed at 623 K for 30 min	2.1	65	1.33

Hydrogenation of the amorphous Y_xFe_{100-x} alloys increases the magnetization and the density of states (Coey *et al* 1988). The abrupt change from a large moment in the ferromagnetic state to a small moment in the antiferromagnetic state takes place at around 0.25 nm for the Fe–Fe interatomic distance in FCC Fe (Wassermann 1990). It has been reported that for amorphous Fe-based alloys the Fe–Fe interatomic distance is very close

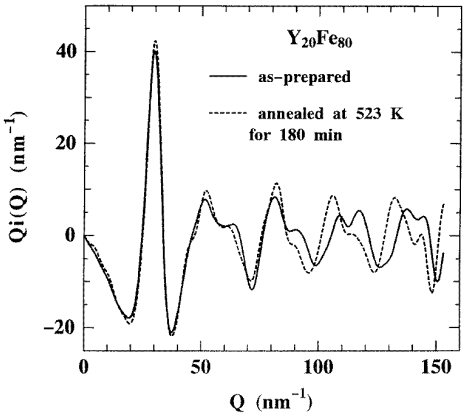

Figure 15. Interference functions of the amorphous $Y_{20}Fe_{80}$ alloys in the as-prepared state and the annealed state at 523 K for 180 min.

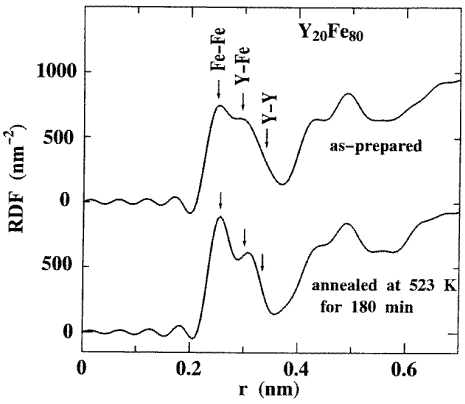

Figure 16. Radial distribution functions (RDFs) for the amorphous $Y_{20}Fe_{80}$ alloys in the as-prepared state and in the annealed state at 523 K for 180 min.

Table 2. The atomic distances r and the coordination numbers N for the $Y_{20}Fe_{80}$ alloys in the as-prepared state and in the annealed state at 523 K for 180 min.

	As prepared		Annealed	
	r (nm)	N	r (nm)	N
Fe–Fe	0.251 ± 0.002	7.5 ± 0.2	0.256 ± 0.002	8.4 ± 0.2
Fe–Y	0.296 ± 0.002	2.6 ± 0.2	0.299 ± 0.002	2.3 ± 0.2
Y–Fe	0.296 ± 0.002	10.5 ± 0.3	0.299 ± 0.002	9.2 ± 0.3
Y–Y	0.336 ± 0.002	6.9 ± 0.3	0.330 ± 0.002	5.8 ± 0.3

to 0.25 nm (Matsuura *et al* 1989), and that for an amorphous YFe_2 alloy it is 0.254 nm (Forester *et al* 1979). Consequently, it is concluded that the increase in the atomic distance of the Fe–Fe pairs from 0.251 to 0.256 nm by annealing stabilizes the ferromagnetic state in the present amorphous $Y_{20}Fe_{80}$ alloy.

Recently, re-entrant spin-glass behaviour has been observed for amorphous Y–Fe alloys prepared by melt-spinning (Tange *et al* 1995). The difference between the magnetic phase diagrams of the melt-spun and sputtered alloys has been attributed to the difference in the quenching speeds, depending on the preparation method (Tange *et al* 1995), namely the degree of atomic disorder is changed by the quenching speed. The present results are explained by assuming that the atomic distance of the Fe–Fe pair after annealing in the sputtered specimen is close to that in the specimen prepared by melt-quenching.

The magnetic properties of amorphous Fe-based alloy should also be discussed in terms of the coordination number of neighbouring Fe atoms, as well as the atomic distance of the Fe–Fe pairs. The relation between coordination number and the magnetic moment on the local Fe site has been discussed by using the data on the Mössbauer effect for the amorphous Y–Fe alloy system (Chappert *et al* 1981). According to those results, the critical coordination number for the onset of the magnetic moment on the Fe site is five and the magnetic moment increases with increasing coordination number up to ten or more. For the amorphous $Y_{20}Fe_{80}$ alloy, the coordination number of the nearest-neighbour Fe atoms increases from 7.5 to 8.4 after annealing, as given in table 2. This change is also

consistent with the increase in the Fe magnetic moment. A slight increase in the atomic distance and/or the coordination number of the Fe–Fe pairs on annealing has also been observed for amorphous $R_{33.3}Fe_{66.7}$ (R = La, Ce or Nd) alloys (Matsubara *et al* 1992). Therefore, it is considered that the atomic distance and the coordination number of the Fe–Fe pairs in the amorphous $Y_{33.3}Fe_{66.7}$ alloy increase after annealing. In the vicinity of this concentration, no ferromagnetic phase appears and the spin freezing temperature increases on annealing, as shown in figure 11. This change is attributed to the increase in both the atomic distance and the coordination number of the Fe–Fe pairs. Because of the itinerant character of 3d electrons of Fe, the local moment on the Fe site fluctuates around the average Fe magnetic moment in amorphous Fe-based alloys. Furthermore, the energy gain of ferromagnetic and antiferromagnetic exchange interactions is closely correlated with the thermal average of amplitude of local moment (Kakehashi 1991), namely the amplitude of the local moment is distributed from zero to a certain large value, and a small local moment couples antiferromagnetically while a large local moment couples ferromagnetically. The average Fe moment would be increased by the structural change in the amorphous $Y_{33.3}Fe_{66.7}$ alloy, and non-magentic Fe sites tend to become antiferromagnetic. On the other hand, the change in the magnetic phase diagram at around 90 at.% Fe should be explained in a different way. In this concentration region, the neighbouring atoms are mostly Fe atoms. The increase in the number of short-range cluster of Fe atoms causes broadening of the Fe 3d electron bands, and hence the frustration becomes stronger (Yu and Kakehashi 1995, Kakehashi and Yu 1995). Therefore, the increase in the spin freezing temperature after annealing would be caused by the clustering of Fe atoms.

4. Conclusions

The annealing effects on the magnetic properties for the amorphous Y_xFe_{100-x} alloys ($x = 7.5$, 10, 15, 16, 20, 25, 30 and 33.3) and on the structural changes for the amorphous $Y_{20}Fe_{80}$ alloy have been investigated. The main results are summarized as follows.

(1) Re-entrant spin-glass behaviour is observed in the annealed amorphous $Y_{15}Fe_{85}$, $Y_{16}Fe_{84}$, $Y_{20}Fe_{80}$, $Y_{25}Fe_{75}$ and $Y_{30}Fe_{70}$ alloys.

(2) The amorphous alloys with low Y concentration such as $Y_{7.5}Fe_{92.5}$ and $Y_{10}Fe_{90}$ and the alloys with a high Y concentration such as $Y_{33.3}Fe_{66.7}$ exhibit the paramagnetic–spin-glass transition even after annealing.

(3) The magnetic phase diagram for the annealed amorphous Y_xFe_{100-x} alloy system is similar to that for many as-prepared amorphous Fe-based alloy systems in a wide concentration range, showing re-entrant spin-glass behaviour.

(4) For the amorphous $Y_{20}Fe_{80}$ alloy, the Curie temperature and the magnetic moment μ_{Fe} increase but the spin freezing temperature decreases on annealing.

(5) The interatomic distance of Fe–Fe pairs and the coordination number of the nearest-neighbour Fe atoms are increased by annealing.

Acknowledgments

Thanks are given to Dr H Komatsu and Dr T H Chiang for their assistance with the sample preparation. The present study has been financed by a Grant-in-Aid for Scientific Research (A) 04402045, from the Japanese Ministry of Education, Science and Culture.

References

Chappert J, Coey J M D, Liénard A and Rebouillat J P 1981 *J. Phys. F: Met. Phys.* **11** 2727–44
Chiang T H, Matsubara E, Kataoka N, Fukamichi K and Waseda Y 1994 *J. Phys.: Condens. Matter* **6** 3457–68
Chudnovsky E M, Saslow W M and Serato R A 1986 *Phys. Rev.* B **33** 251–61
Coey J M D, Givord D, Liénard A and Rebouillat J P 1981 *J. Phys. F: Met. Phys.* **11** 2707–25
Coey J M D, Liénard A, Rebouillat J P, Ryan D H, Zhenxi Wang and Boliang Yu 1988 *J. Phys. F: Met. Phys.* **18** 1299–310
Fähnle M and Kronmüller H 1978 *J. Magn. Magn. Mater.* **8** 149–56
Forester D W, Koon N C and Schelleng J H 1979 *J. Appl. Phys.* **50** 7336–41
Fujita A, Komatsu H, Fukamichi K and Goto T 1993 *J. Phys.: Condens. Matter* **5** 3003–10
Fujita A, Suzuki T, Kataoka N and Fukamichi K 1994 *Phys. Rev.* B **50** 6199–202
Fukamichi K, Chiang T H, Fujita A, Tange H, Kawabuchi S and Ono T 1995 *J. Phys.: Condens. Matter* **7** 2875–87
Fukamichi K, Goto T, Komatsu H and Wakabayashi H 1989 *Proc. 4th Int. Conf. on Phys. Magn. Mater. (Szczyrk-Biła, 4–10 September 1988)* (Singapore: World Scientific) pp 354–80
Fukamichi K, Hiroyoshi H, Shirakawa K, Masumoto T and Kaneko T 1986 *IEEE Trans. Magn.* **22** 424–6
Hiroyoshi H, Noguchi K, Fukamichi K and Nakagawa Y 1985 *J. Phys. Soc. Japan* **54** 3554–61
Kakehashi Y 1991 *Phys. Rev.* B **43** 10 820–31
——1993 *Phys. Rev.* B **47** 3185–95
Kakehashi Y and Yu M 1995 *J. Magn. Magn. Mater.* **140–144** 263–4
Matsubara E, Waseda Y, Chiang T H and Fukamichi K 1992 *J. Mater. Sci. Lett.* **11** 1521–4
Matsuura M, Wakabayashi H, Goto T, Komatsu H and Fukamichi K 1989 *J. Phys.: Condens. Matter* **1** 2077–86
Rao N V, Reddy S B, Satyanarayana G and Sastry D L 1986 *Physica* C **138** 215–18
Suzuki T, Fujita A, Chiang T H and Fukamichi K 1994a *Mater. Eng. Sci.* A **181–182** 954–7
Suzuki T, Fujita A, Fukamichi K and Goto T 1994b *J. Phys.: Condens. Matter* **6** 5741–50
Tange H, Ikeda M, Ono T, Kamimori T and Goto M 1995 *J. Magn. Magn. Mater.* **140–144** 287–8
Terashima S, Fukamichi K, Goto T, Chiang T H, Mastubara E and Waseda Y 1996 *J. Phys.: Condens. Matter* **8** 2053
Wakabayashi H, Goto T, Fukamichi K and Komatsu H 1990 *J. Phys.: Condens. Matter* **2** 417–29
Wassermann E F 1990 *Ferromagnetic Materials* vol 5, ed K H J Buschow and E P Wohlfarth (Amsterdam: North-Holland) pp 237–322
Yu M and Kakehashi Y 1995 *J. Magn. Magn. Mater.* **140–144** 289–90